LETTERS

Variable Quaternary chemical weathering fluxes and imbalances in marine geochemical budgets

Derek Vance[1], Damon A. H. Teagle[2] & Gavin L. Foster[1]

Rivers are the dominant source of many elements and isotopes to the ocean. But this input from the continents is not balanced by the loss of the elements and isotopes through hydrothermal and sedimentary exchange with the oceanic crust, or by temporal changes in the marine inventory for elements that are demonstrably not in steady state[1–4]. To resolve the problem of the observed imbalance in marine geochemical budgets, attention has been focused on uncertainties in the hydrothermal and sedimentary fluxes[1–4]. In recent Earth history, temporally dynamic chemical weathering fluxes from the continents are an inevitable consequence of periodic glaciations[5–9]. Chemical weathering rates on modern Earth are likely to remain far from equilibrium owing to the physical production of finely ground material at glacial terminations[10–13] that acts as a fertile substrate for chemical weathering. Here we explore the implications of temporal changes in the riverine chemical weathering flux for oceanic geochemical budgets. We contend that the riverine flux obtained from observations of modern rivers is broadly accurate, but not representative of timescales appropriate for elements with oceanic residence longer than Quaternary glacial–interglacial cycles. We suggest that the pulse of rapid chemical weathering initiated at the last deglaciation has not yet decayed away and that weathering rates remain about two to three times the average for an entire late Quaternary glacial cycle. Taking into account the effect of the suggested non-steady-state process on the silicate weathering flux helps to reconcile the modelled marine strontium isotope budget with available data. Overall, we conclude that consideration of the temporal variability in riverine fluxes largely ameliorates long-standing problems with chemical and isotopic mass balances in the ocean.

For many elements and isotopes, the riverine flux is the dominant input to the oceans and is at least partially balanced by outputs to—or exchange with—the oceanic crust, either via alteration of basalts or deposition in sediments[1–4]. For some elements with isotopic systems, such as strontium (Sr) and osmium (Os), the oceans are demonstrably not in perfect steady state[14,15]. For example, for the past few million years the oceanic $^{87}Sr/^{86}Sr$ ratio has been rising at a rate of $0.000054\,Myr^{-1}$. Therefore, the input of relatively radiogenic Sr from the continents cannot be perfectly balanced by unradiogenic Sr derived from hydrothermal exchange with the oceanic crust[3,16], which for many elements is the second greatest influence on seawater chemistry after rivers[1]. The extent of Sr isotopic alteration of oceanic crust in drill cores and ophiolites[3] implies a high-temperature hydrothermal fluid flux of around $(0.5–3) \times 10^{13}\,kg\,yr^{-1}$ (Fig. 1). This estimate agrees well with those obtained from a range of other elements in altered oceanic crust and overlaps with those from thermal calculations (Fig. 1). But, when combined with the modern measured riverine Sr flux (Supplementary Table 1), such a hydrothermal flux would suggest that seawater $^{87}Sr/^{86}Sr$ should be evolving at a rate of $0.000425\,Myr^{-1}$, eight times faster than implied by the record of Sr isotopes in sea water[14]. To keep the Sr isotope ratio of sea water evolving at the slow rate which the records suggest, the flux of water through high-temperature hydrothermal systems would need to be $>10^{14}\,kg\,yr^{-1}$ (Supplementary Table 2), in marked contrast to the consensus from observations of the alteration state of the oceanic crust for a range of elements and isotope systems (Fig. 1). This problem with marine geochemical budgets is by no means unique to Sr. For Mg, another element whose marine geochemistry is the basis of a prominent palaeoceanographic tool, rivers are also the main input and hydrothermal systems are an important sink[4,17]. The Mg budget of the oceans is also demonstrably out of steady state[4,17], but even the inclusion of a secular increase in oceanic Mg concentrations through time cannot balance the budget.

To resolve these issues, attention has traditionally focused on uncertainties in hydrothermal fluxes. After all, the riverine input flux is directly and comprehensively observable. Pollution of modern

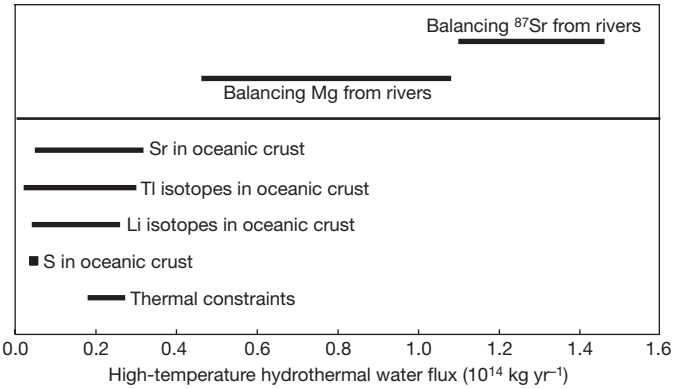

Figure 1 | Estimates of the hydrothermal water flux at mid-ocean ridges. Shown is a comparison of estimates of the high-temperature hydrothermal water flux obtained from a range of observations of the oceanic crust (bottom panel) with those required by the need to balance the riverine input of Mg and radiogenic Sr from the continents (top panel). The range of hydrothermal water fluxes required to balance radiogenic Sr in rivers is derived from calculations in Supplementary Tables 2 and 3. These are a factor of 4–20 higher than is permitted by constraints deriving from the alteration state of the oceanic crust for Sr isotopes[3,28]. Analogous constraints from Mg are looser, and the range for the requirement imposed by the riverine input reflects uncertainty over the extent of steady state in the ocean for Mg and debate over the size of outputs from the oceans other than high-temperature hydrothermal systems[4,17]. Overall, the geochemical (Li and Tl isotopes, elemental S) and geophysical (data compiled in refs 28, 29) constraints on the size of the high-temperature hydrothermal flux from the oceanic crust are rather concordant, at $(0.1–0.2) \times 10^{13}\,kg\,yr^{-1}$, and stand in marked contrast to the factor ~10 higher value required by the riverine flux of Sr to the oceans.

[1]Bristol Isotope Group, Department of Earth Sciences, University of Bristol, Wills Memorial Building, Bristol BS8 1RJ, UK. [2]School of Ocean and Earth Science, National Oceanography Centre, University of Southampton, Southampton SO14 3ZH, UK.

rivers is significant for many elements but not for the main cations at the magnitude of interest here[18]. A potentially more serious issue is the inherent temporal variability of rivers[2,16], and the possibility that the extensive database for Sr and its isotopes in modern rivers does not accurately yield a global Sr flux to the oceans. However, although major rivers show pronounced seasonality, recent data suggest that the required hydrothermal flux is sensitive only at the 10–15% level to plausible variations in the global riverine flux (Supplementary Tables 1 and 2). The initial conclusion, that the modern riverine Sr flux requires an unrealistically high hydrothermal flux ($>10^{14}$ kg yr^{-1}), around an order of magnitude higher than independent estimates, therefore appears robust. We contend that the riverine flux obtained from observations of modern rivers is broadly accurate, but that it is not representative of timescales of 10^5–10^7 years, those appropriate for an element with an oceanic residence time much longer than Quaternary glacial–interglacial cycles.

About 25–30% of the currently ice-free continental area was covered by large ice sheets during the Quaternary glacial periods, including the Last Glacial Maximum 18 kyr ago[19]. Chemical weathering rates underneath the dry-based late Quaternary ice sheets were near negligible[20]. In contrast, glacial and ice sheet physical weathering rates are very high[10,20]; they are estimated to be 10 times greater than without Northern Hemisphere glaciation[10]. The demise of the continental ice sheets at glacial terminations leaves behind large amounts of fresh, finely ground rock in young moraines and soils that provide fertile substrates for chemical weathering. High deglacial physical weathering rates are not confined to high latitudes. In the European Alps, a 12–20-fold increase in sediment delivery to peri-Alpine valleys and lakes[13] occurred 17–11 kyr ago, and is related to dispersal of glacially-ground sediment due to increased melt water and wetter conditions immediately post-glacial. Huge amounts of sediment were delivered to the Ganges flood-plain from the Himalaya between 11 and 7 kyr ago[12], with sediment storage increasing 10 times. This latter phenomenon was driven by the early Holocene peak in monsoonal precipitation[12], rather than changes in glacial coverage, and there is evidence for a global expression of this phenomenon in the period after about 10 kyr ago[11].

Field and laboratory observations suggest that newly produced fine-grained material is highly reactive when initially exposed to agents of chemical weathering, but that rates decrease dramatically with time (Fig. 2). The slope of the power law relationship between weathering rate and exposure time for post-glacial soils[5] is similar to that obtained from laboratory experiments on Panola granite[21] and to recent field studies of Hawaiian basalt flows[22] (Fig. 2). It is important to note that for both granitic and basaltic lithologies, and for climatic regimes ranging from cold to tropical, the dependence of weathering rate on substrate age is the same, despite variations in absolute weathering rate. These experiments and observations refer only to silicates. In principle, similar processes could occur with carbonate weathering, but the orders of magnitude faster reaction kinetics for calcite dissolution relative to silicates[20] suggest that carbonate dissolution is much closer to keeping pace with physical grinding. Here we follow others[19] in assuming that carbonate weathering rates remain more or less constant (except on carbonate shelves exposed during sea-level low-stands: see below), and keep pace with environmental change, through glacial–interglacial cycles.

Using the relationship between soil age and silicate weathering rate (Fig. 2), we can estimate the effect of increased high-latitude chemical weathering over the last glacial cycle (Fig. 3a). This indicates that the pulse of rapid chemical weathering initiated at the last deglaciation (18 kyr ago) has not yet decayed away and rates remain about twice the average for an entire late Quaternary glacial cycle. This is supported by measured weathering rates in the drainage basins of two major Canadian rivers, the Mackenzie and the St Lawrence[23], whose dissolved load suggests a modern weathering rate that is 3–4 times higher than the long-term model rate.

These high modern, relative to long-term, weathering rates are also supported by a range of studies on the modern chemistry of major

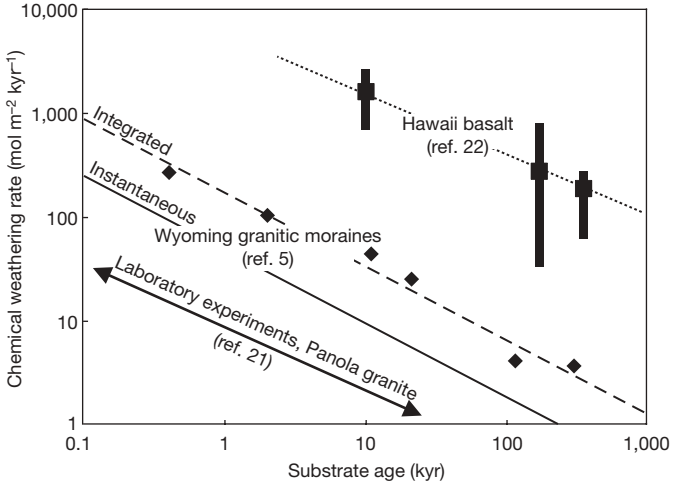

Figure 2 | Dependence of chemical weathering on substrate age. Diamonds, measured chemical depletion rates for a sequence of soils developed on moraines of varying age deposited by retreating glaciers/ice-sheets in Wyoming[5]. The data conform to a power law relationship, with instantaneous weathering rate at any time t subsequent to exposure from beneath the ice being given by the solid line ($50t^{-0.71}$). Laboratory data on the weathering rate of Panola granite[21] (double-headed arrow, absolute rates depend on starting experimental surface area, exponent = −0.61), as well as recent data for a series of Hawaiian basaltic lavas[22] (averages and ranges across a range of precipitation conditions given by squares and vertical bars, exponent = −0.61) yield relationships between time-integrated weathering rate and substrate age that are very similar to the Wyoming data. The similarity in the slopes of these relationships suggests a dependence of weathering rate on substrate age that is common across climatic regimes and silicate lithologies, despite a two orders of magnitude variation in absolute weathering rates that is dependent on climate and lithology.

drainage basins, particularly U–Th isotope investigations that often point to departures from steady state in the past 5–20 kyr (data compiled in ref. 9). Moreover, oceanic Pb isotopes have recently provided further support for substantial glacial–interglacial changes in silicate weathering on the continents[8]. Other evidence substantiates suggestions of non-steady-state chemical weathering in some drainage basins not directly affected by glaciation[9]. U–Th isotopes in rivers draining the Andes have, for example, been out of steady state for between 4 and 20 kyr (ref. 9). The exact magnitude of continued departure from steady state in these mountainous regions is important because of their importance to total riverine fluxes[24], but is much more difficult to quantify than for high latitudes. Furthermore, it is also clear that some lowland tropical rivers are close to steady state at the present day[9]. Nonetheless, the similarity in the form of Fig. 3a and the records of sediment production in the European Alps and the Himalaya (Fig. 3b) is striking, and supports the notion that a late deglacial pulse of sediment generation also occurred in these mountainous regions.

Figure 4 investigates the impact on the marine Sr isotope budget of the suggestion that present-day Sr fluxes are out of steady state (see Supplementary Information for model details). In addition to the changes in the silicate weathering flux detailed above, our calculations also take into account well-documented effects arising from the incongruent release of radiogenic Sr early in the weathering process (see Supplementary Information for details). As with Pb isotopes[7,8], young soils preferentially release highly radiogenic Sr during initial weathering[6], and the co-release of the radiogenic Pb (ref. 8) and Sr is supported by granitoid leaching experiments (Supplementary Information).

Figure 4 compares outputs of models of deglacial weathering with high resolution measurements of Sr isotopes in foraminiferal carbonate over the past 400 kyr (ref. 25). The isotope record places tight limits on the Sr isotopic evolution of sea water and the amplitude of

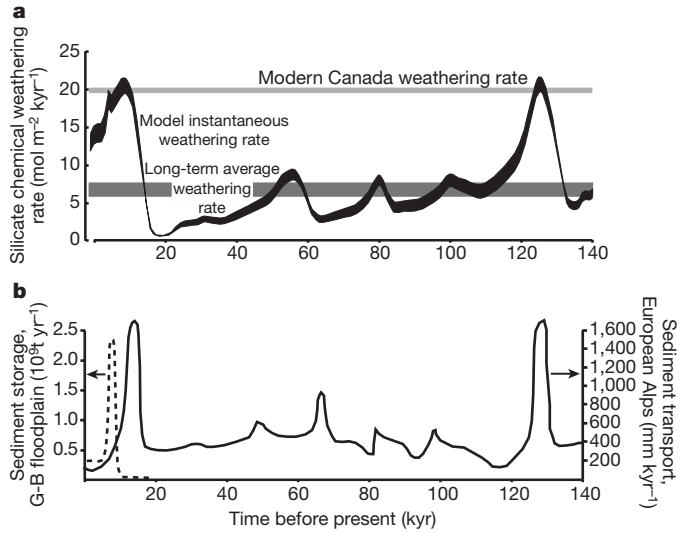

Figure 3 | Chemical and physical weathering rates over the last glacial cycle. **a**, Model of instantaneous silicate chemical weathering rate (black curve) in the 25–30% (ref. 19) of the extra-Antarctic continent that was glaciated at some point over the last glacial cycle, using the relationships between soil age and weathering rate from Fig. 1 and ice-sheet coverage forced by marine oxygen isotope data (see Supplementary Information for details). At deglaciations, for example, the last starting approximately 18 kyr ago, weathering rates rise rapidly as pristine soil parent material is exposed from underneath the retreating ice-sheet. The rate then decays away during the subsequent interglacial as this material ages (Fig. 2), but present-day weathering rates are still modelled to be about a factor of two higher than the rate over an entire glacial cycle (lower, darker-grey band). The ranges in both this long-term and the instantaneous weathering rates (the thickness of the bands) are given by assuming the range of exponential dependencies of weathering rate on time seen in Fig. 2. The upper, lighter-grey band gives the average (weighted according to drainage basin area) of the silicate weathering rates estimated for the Mackenzie and St Lawrence river basins at the present day[23]. **b**, Production of new sediment in peri-Alpine basins over the last glacial cycle (solid curve, right axis, expressed as an equivalent denudation rate for the mountain belt as in the original paper[13]) and sediment storage in the Ganges-Brahmaputra (G-B) floodplain (dashed line, left axis[12]) over the last deglaciation. These changes in sediment supply would produce pulses in chemical weathering rate very similar to those modelled for the high-latitude glaciated regions in **a**.

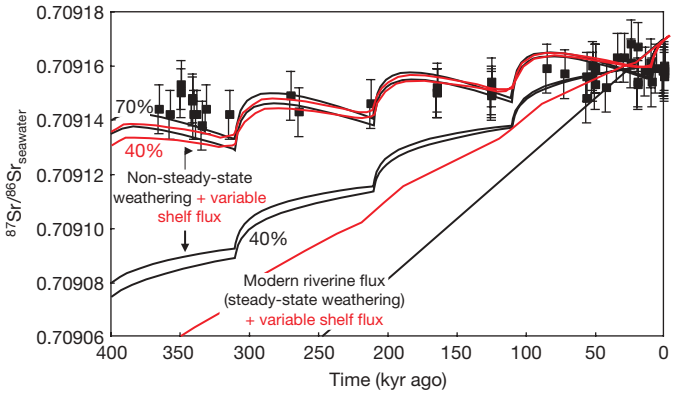

Figure 4 | Sr behaviour during weathering and the oceanic mass balance. The evolution of $^{87}Sr/^{86}Sr$ in the oceans from records in marine carbonate[25] (filled squares; error bars represent 95% confidence intervals) compared to those produced by model simulations. The two lines labelled 'modern riverine flux (steady-state weathering)' assume a Sr flux and isotopic composition from the continental crust as given by the modern riverine flux with (red) or without (black) a maximum increased flux of unradiogenic Sr from carbonate shelves during glacial sea-level low-stands[30], and suggest an evolution that is 6–8 times faster than observed. On the other hand, if 40–70% of the silicate weathering flux is subject to non-steady-state weathering caused by variable substrate ages, the models are consistent with data. In the models (see Supplementary Information for details), the specified portion of the silicate weathering flux is affected by variable substrate ages through time (Fig. 3), such that weathering rates are reset to high values by young substrates produced at deglaciations. The weathering flux of Sr is also affected by substrate-age-dependent incongruent weathering of Sr isotopes. The two curves for each percentage are for different degrees of incongruent weathering of Sr isotopes at the present day, such that $^{87}Sr/^{86}Sr$ weathered from modern soils is 1.002 and 1.004 times the bulk soil value (or 0.2% and 0.4% higher than the bulk soil; see ref. 6, main text and Supplementary Information).

variations. Figure 4 demonstrates once again that if the modern riverine flux of Sr and its isotopes is representative of the long-term flux, then sea water evolves in $^{87}Sr/^{86}Sr$ much more rapidly than the data allow. The modelled rate of evolution in seawater Sr isotopes matches data more closely, given maximum allowable changes in the flux of unradiogenic Sr from shelf carbonates during the sea-level low-stands of glacial periods (see Supplementary Information for details), but is still a factor of six too fast. However, if about 70% of the silicate weathering flux is affected by non-steady-state processes, the modelled evolution of sea water matches the data over the long term. Alternatively, a lower limit of 40% of the silicate chemical weathering flux affected by the processes is permitted if maximum increases in the unradiogenic flux from carbonates during glacial sea-level low-stands are allowed. Our weathering scenario produces cyclicity in the Sr isotopic composition of sea water, such that deglaciations are characterized by rapid (~10 kyr) increases in $^{87}Sr/^{86}Sr$, followed by slow (~90 kyr) reductions. The cyclicity generated, however, is not inconsistent with the best data we currently have for Sr isotopes in the oceans over the past 400 kyr (ref. 25).

The above ideas, successful for Sr, have implications for the oceanic budgets of other elements, whose quantitative validity might be tested in the future. First, our weathering scenario could explain similar imbalances in the marine geochemical budgets of other elements with long oceanic residence times. The modern riverine input of Mg, even when a secular increase in oceanic concentrations is taken into account[4], is also much greater than the current best estimates of the outputs[4,17]. As a consequence of its long ocean residence time (10 Myr) and the dominance of slow pre-Quaternary rates in the long-term average[19], the modern supply of Mg to the oceans is even further out of step than Sr with the relevant long-term value. The assessment of the quantitative impact of this assertion is complicated by major uncertainty in the fraction of the riverine Mg budget that derives from silicate weathering (21–54%; ref. 18) and additional uncertainties over the long-term magnitude of key output fluxes, such as those to dolomite or to basalts[4,17]. Such uncertainties at present preclude the use of the Mg budget to test the hypothesis of non-steady-state weathering, but our models do represent a target for improved information on the global budget of Mg that is likely to emerge in the near future from its nascent isotope system[17].

Second, for elements with an isotope system and whose residence times are sufficiently short to resolve glacial–interglacial changes in the weathering flux, we predict discernible glacial–interglacial cyclicity in their oceanic isotope geochemistry.

In addition to Pb, the oceanic behaviour of which has already been shown to be consistent with our ideas[8], Os is another element for which glacial–interglacial cycles in its seawater isotopic composition are well established[15]. These changes are attributed to changes in the flux of radiogenic Os from the continents resulting from low weathering rates during glacial periods. However, modelling of Os isotopes purely in terms of lower weathering fluxes during glacial periods has shown that the glacial–interglacial changes can only be explained with an oceanic residence time for Os near 3 kyr (ref. 15), inconsistent with the much longer residence time (35–50 kyr) suggested by the small contrast in the Os isotopic compositions of different ocean basins. The only way to explain the glacial–interglacial changes with the longer residence

times is to invoke a transient Os spike at deglaciations due to rapid weathering of glacial till[15], in direct congruence with the processes invoked here. Furthermore, previous work on the marine Os cycle has not considered possible changes in the isotopic composition of the riverine flux. Os is affected by exactly the same processes that affect the isotopic composition of Sr released in the weathering environment, with young soils releasing highly radiogenic Os and freshwater Fe-Mn nodules in post-glacial lakes containing extreme Os isotope compositions[26].

Though not directly addressed here, our ideas invoking faster deglacial weathering rates would drive atmospheric CO_2 downwards by 10–20 p.p.m. when ice cores record a rise at deglaciations[27]. A full assessment of the magnitude of this phenomenon must await a comprehensive carbon cycle model, including a determination of the timing of predicted pulses in silicate weathering in the glaciated regions in response to ice-sheet retreat early in a deglaciation versus a later pulse in response to a strong early Holocene monsoon. A corollary to the ideas presented here (see also ref. 19) is that long-term CO_2 drawdown in an ice-house world such as the Quaternary—with cycles of physical (glacial) grinding making material available for subsequent intense chemical (interglacial) weathering—is faster than in the absence of these climate changes. The implication is that the CO_2–weathering feedback is weakened (and perhaps even changed in sign) during periods like the Quaternary, perhaps contributing to the maintenance of ice-house conditions once they are initiated.

Received 17 July 2008; accepted 22 January 2009.

1. Elderfield, H. & Schultz, A. Mid-ocean hydrothermal fluxes and the chemical composition of the ocean. *Annu. Rev. Earth Planet. Sci.* **24,** 191–224 (1996).
2. Galy, A., France-Lanord, C. & Derry, L. A. The strontium isotopic budget of Himalayan rivers in Nepal and Bangladesh. *Geochim. Cosmochim. Acta* **63,** 1905–1925 (1999).
3. Davis, A. C., Bickle, M. J. & Teagle, D. A. H. Imbalance in the oceanic strontium budget. *Earth Planet. Sci. Lett.* **211,** 173–187 (2003).
4. Holland, H. D. Sea level, sediments and the composition of seawater. *Am. J. Sci.* **305,** 220–239 (2005).
5. Taylor, A. & Blum, J. D. Relation between soil age and silicate weathering rates determined from the chemical evolution of a glacial chronosequence. *Geology* **23,** 979–982 (1995).
6. Blum, J. D. & Erel, Y. Rb-Sr isotope systematics of a granitic soil chronosequence: The importance of biotite weathering. *Geochim. Cosmochim. Acta* **61,** 3193–3204 (1997).
7. Harlavan, Y., Erel, Y. & Blum, Y. D. Systematic changes in lead isotopic composition with soil age in glacial granitic terrains. *Geochim. Cosmochim. Acta* **62,** 33–46 (1998).
8. Foster, G. L. & Vance, D. Negligible glacial-interglacial variation in continental chemical weathering rates. *Nature* **444,** 918–921 (2006).
9. Dosseto, A., Bourdon, B. & Turner, S. P. Uranium-series isotopes in river materials: Insights into the timescales of erosion and sediment transport. *Earth Planet. Sci. Lett.* **265,** 1–17 (2008).
10. Bell, M. & Laine, E. P. Erosion of the Laurentide region of North America by glacial and glaciofluvial processes. *Quat. Res.* **23,** 154–174 (1985).
11. Thomas, M. F. & Thorp, M. B. Geomorphic response to rapid climatic and hydrologic change during the late Pleistocene and early Holocene in the humid and sub-humid tropics. *Quat. Sci. Rev.* **14,** 193–197 (1995).
12. Goodbred, S. L. Jr & Kuehl, S. A. Enormous Ganges-Brahmaputra sediment discharge during strengthened early Holocene monsoon. *Geology* **28,** 1083–1086 (2000).
13. Hinderer, M. Late Quaternary denudation of the Alps, valley and lake fillings and modern river loads. *Geodinam. Acta* **14,** 231–263 (2001).
14. Hodell, D. A., Mueller, P. A., McKenzie, J. A. & Mead, G. A. Strontium isotope stratigraphy and geochemistry of the late Neogene ocean. *Earth Planet. Sci. Lett.* **92,** 165–178 (1989).
15. Oxburgh, R., Pierson-Wickmann, A.-C., Reisberg, L. & Hemming, S. Climate-correlated variations in seawater $^{187}Os/^{188}Os$ over the past 200,000 yr: Evidence from the Cariaco Basin, Venezuela. *Earth Planet. Sci. Lett.* **263,** 246–258 (2007).
16. Palmer, M. R. & Edmond, J. M. The strontium isotope budget of the modern ocean. *Earth Planet. Sci. Lett.* **92,** 11–26 (1989).
17. Tipper, E. T. *et al.* The magnesium isotope budget of the modern ocean: Constraints from riverine magnesium isotope ratios. *Earth Planet. Sci. Lett.* **250,** 241–253 (2006).
18. Gaillardet, J., Dupré, B., Louvat, P. & Allègre, C. J. Global silicate weathering and CO_2 consumption rates deduced from the chemistry of large rivers. *Chem. Geol.* **159,** 3–30 (1999).
19. Clark, P. U. *et al.* The middle Pleistocene transition: Characteristics, mechanisms and implications for long-term changes in atmospheric CO_2. *Quat. Sci. Rev.* **25,** 3150–3184 (2006).
20. Anderson, S. P. Biogeochemistry of glacial landscape systems. *Annu. Rev. Earth Planet. Sci.* **35,** 375–399 (2007).
21. White, A. F. & Brantley, S. L. The effect of time on the weathering of silicate minerals: Why do weathering rates differ in the laboratory and the field? *Chem. Geol.* **202,** 479–506 (2003).
22. Porder, S., Hilley, G. E. & Chadwick, O. A. Chemical weathering, mass loss, and dust inputs across a climate by time matrix in the Hawaiian Islands. *Earth Planet. Sci. Lett.* **258,** 414–427 (2007).
23. Millot, R., Gaillardet, J., Dupré, B. & Allègre, C. J. The global control of silicate weathering rates and the coupling with physical erosion: New insights from rivers of the Canadian Shield. *Earth Planet. Sci. Lett.* **196,** 83–98 (2002).
24. West, A. J., Galy, A. & Bickle, M. Tectonic and climatic controls on silicate weathering. *Earth Planet. Sci. Lett.* **235,** 211–228 (2005).
25. Henderson, G. M., Martel, D. J., O'Nions, R. K. & Shackleton, N. J. Evolution of seawater $^{87}Sr/^{86}Sr$ over the last 400 ka: The absence of glacial/interglacial cycles. *Earth Planet. Sci. Lett.* **128,** 643–651 (1994).
26. Peucker-Ehrenbrink, B. & Blum, J. D. Re-Os isotope systematics and weathering of Precambrian crustal rocks: Implications for the marine osmium isotope record. *Geochim. Cosmochim. Acta* **62,** 3193–3203 (1998).
27. Petit, J. R. *et al.* Climate and atmospheric history of the past 420,000 years from the Vostok ice core, Antarctica. *Nature* **399,** 429–436 (1999).
28. Teagle, D. A. H., Bickle, M. J. & Alt, J. C. Recharge flux to ocean-ridge black smoker systems: A geochemical estimate from ODP Hole 504B. *Earth Planet. Sci. Lett.* **210,** 81–89 (2003).
29. Nielsen, S. G. *et al.* Hydrothermal fluid fluxes calculated from the isotopic mass balance of thallium in the ocean crust. *Earth Planet. Sci. Lett.* **251,** 120–133 (2006).
30. Stoll, H. M. & Schrag, D. P. Effect of Quaternary sea-level cycles on Sr in seawater. *Geochim. Cosmochim. Acta* **62,** 1107–1118 (1998).

Supplementary Information is linked to the online version of the paper at www.nature.com/nature.

Acknowledgements We thank H. Pälike, M. Palmer, C. Hawkesworth, T. Elliott, D. Schmidt, M. Gutjahr and M. Andersen for reading and improving an earlier version of this paper, and J. Phillips for help with a statistics problem. This work was done while D.V. held a Blaustein Visiting Research Professorship at Stanford.

Author Information Reprints and permissions information is available at www.nature.com/reprints. Correspondence and requests for materials should be addressed to D.V. (d.vance@bristol.ac.uk).

SUPPLEMENTARY INFORMATION

Table S1: Compilation of Sr isotope compositions[1,2,3] and Sr fluxes from major world rivers, updated from those in references 1 and 2.

River	Sr (μmol/kg)	$^{87}Sr/^{86}Sr$	Discharge[4] (km^3/yr)	Sr flux[5] (mol/yr)	Source
Amazon	0.26	0.7112	6590	$1.68x10^9$	Average refs 1 and 2.
Indonesian rivers	**0.30**	**0.7083**	**1734**	**$5.20x10^8$**	**Estimate in ref 1.**
Zaire	0.23	0.7173	1200	$2.76x10^8$	Average refs 1 and 2.
Orinoco	0.21	0.7183	1135	$2.38x10^8$	1
Chang Jiang (Yangtze)	2.24	0.7108	928	$2.07x10^9$	Average refs 1 and 2.
Ganges-Brahmaputra		0.7295	1003	$6.50x10^8$	3
Meghna[6]	0.23	0.7161	162	$3.73x10^7$	4
Mississippi	1.71	0.7102	580	$9.92x10^8$	1
Japan	0.63	0.7076	550	$3.47x10^8$	1
Lena	1.10	0.7048	525	$5.78x10^8$	5
Tocantins	0.32	0.7188	372	$1.17x10^8$	Average refs 1 and 2.
Xingu	0.16	0.7292	505	$8.08x10^7$	1
Tapajos	0.10	0.7322	489	$4.89x10^7$	1
Parana	0.52	0.7139	568	$2.95x10^8$	1
Irrawady[7]	3.39	0.7101	486	$1.65x10^9$	4
Mekong	3.39	0.7102	467	$1.58x10^9$	1
Philippines	1.41	0.7056	332	$4.68x10^8$	1
Pearl (Xijang)	1.02	0.7113	363	$3.70x10^8$	Average refs 1 and 2.
Indus	3.33	0.7112	90	$3.00x10^8$	1
Zambeze	**1.20**	**0.7160**	**224**	**$2.69x10^8$**	**Estimate in ref 1.**
Salween[7]	3.39	0.7099	211	$7.15x10^8$	4
Danube	2.76	0.7089	207	$5.71x10^8$	1
Niger	0.25	0.7140	154	$3.85x10^7$	1
Sao Francisco	**0.25**	**0.7170**	**160**	**$4.00x10^7$**	**Estimate in ref 1.**
Kolyma	0.75	0.7090	132	$9.90x10^7$	5
Hong (Red)	1.30	0.7124	123	$1.60x10^8$	7
Narmada[6]	1.29	0.7125	98	$1.26x10^8$	4
Mozambique	**1.20**	**0.7160**	**85**	**$1.02x10^8$**	**Estimate in ref 1.**
Rhine	6.23	0.7092	69.4	$4.32x10^8$	1
Indigirka	0.82	0.7097	61	$5.00x10^7$	5
Anadyr	0.35	0.7047	60	$2.10x10^7$	5
Rhone	5.94	0.7087	55	$3.27x10^8$	1
Victoria Nile	1.10	0.7114	54	$5.94x10^7$	1
Yellow (Huanghe)	10.23	0.7111	41	$4.19x10^8$	Average refs 1 and 2.
Dniepr	**2.50**	**0.7084**	**43**	**$1.08x10^8$**	**Estimate in ref 1.**
Tanzania	**0.49**	**0.7219**	**38**	**$1.86x10^7$**	**Estimate in ref 1.**
Yana	0.99	0.7099	34	$3.37x10^7$	5
Murray	2.45	0.7108	32	$7.84x10^7$	1
Garonne	1.27	0.7106	28	$3.56x10^7$	1
Don	2.50	0.7084	26	$6.50x10^7$	**Estimate in ref 1.**
Chao Praya	1.07	0.7138	23	$2.46x10^7$	1
Blue Nile	1.55	0.7056	19	$2.95x10^7$	1
Tisza	2.04	0.7096	19	$3.88x10^7$	1
Seine	3.84	0.7082	12.9	$4.95x10^7$	1
Juba	**1.50**	**0.7061**	**17**	**$2.55x10^7$**	**Estimate in ref 1.**
Colorado	13.25	0.7108	13	$1.72x10^8$	1
Mae Klong	0.76	0.7164	13	$9.88\ x10^6$	1
Eel	3.69	0.7064	10	$3.69x10^7$	1
Brazos	6.42	0.7087	10	$6.42x10^7$	1
Orange	1.85	0.7146	10	$1.85x10^7$	1
Manning	1.02	0.7063	9	$9.18x10^6$	1
Maas	2.51	0.7085	8	$2.01x10^7$	1
Kenya	**1.10**	**0.7114**	**6**	**$6.60x10^6$**	**Estimate in ref 1.**
Cauveri	3.62	0.7130	21	$7.60x10^7$	1
Rio Grande	3.25	0.7092	2	$6.50x10^6$	1
Schelde	5.07	0.7088	2	$1.01x10^7$	1
Murchison	12.33	0.7280	0.3	$3.70\ x10^6$	1
Total non-glaciated[8]		**0.71134**	**20210**	**$1.67x10^{10}$**	**77% of global Sr flux**

River	Sr (μmol/kg)	$^{87}Sr/^{86}Sr$	Discharge[4] (km^3/yr)	Sr flux[5] (mol/yr)	Source
Yenisei[9]	**1.43**	**0.7123**	**620**	**$8.87x10^8$**	**8**
Ob[9]	**1.43**	**0.7123**	**404**	**$5.78x10^8$**	**8**
Baltic rivers	1.43	0.7123	443.7	$6.34x10^8$	8
St Lawrence	1.48	0.7096	337	$4.99x10^8$	Average refs 1 and 2.
Mackensie	2.37	0.7112	308	$7.30x10^8$	Average refs 1 and 2.
Yukon	1.59	0.7137	200	$3.18x10^8$	1
Columbia	0.98	0.7121	236	$2.31x10^8$	1
Red	1.50	0.7114	123	$1.85x10^8$	1
Fraser	0.85	0.7116	112	$9.55x10^7$	Average refs 1 and 9.
Churchill	0.08	0.7176	70	$5.60x10^6$	1
Nelson	0.86	0.7146	89.3	$7.68x10^7$	1
Koksoak	0.17	0.7301	52	$8.84x10^6$	1
Saguenay	0.23	0.7131	43	$9.68x10^6$	Average refs 1 and 9.
Kuskokwin	1.33	0.7090	60	$7.98x10^7$	Average refs 1 and 2.
Susquehanna	1.26	0.7142	36	$4.54x10^7$	1
Nottaway	0.13	0.7186	33	$4.29x10^6$	1
Copper	1.45	0.7071	31	$4.50x10^7$	1
Rupert	0.08	0.7283	28	$2.24x10^6$	1
Manicouagan	0.14	0.7169	27	$3.78x10^6$	1
Weser	8.23	0.7089	10.6	$8.72x10^7$	1
St. John	0.67	0.7098	26	$1.74x10^7$	1
Skeena	0.81	0.7046	26	$2.11x10^7$	1
Elbe	6.53	0.7097	22.8	$1.49x10^8$	1
Nass	1.11	0.7054	26	$2.89x10^7$	1
La Grande	0.14	0.7346	24	$3.36x10^6$	1
Stikine	0.66	0.7054	24	$1.58x10^7$	1
Albany	0.32	0.7158	23	$7.36x10^6$	1
Eastmain	0.07	0.7285	22	$1.54x10^6$	1
Severn	0.39	0.7182	21	$8.19x10^6$	1
Aux Feuilles	0.11	0.7347	20	$2.20x10^6$	1
St. Maurice	0.15	0.7117	19	$2.76x10^6$	Average refs 1 and 9.
Moose	0.48	0.7132	19	$9.12x10^6$	1
A La Baleine	0.16	0.7265	19	$3.04x10^6$	1
Gde Riv de la Baleine	0.10	0.7384	16	$1.60x10^6$	1
Petit Mecatina	0.15	0.7105	16	$2.40x10^6$	1
Churchill M	0.26	0.7200	16	$4.16x10^6$	1
Back	0.09	0.7291	16	$1.44x10^6$	1
Dvina	**2.50**	**0.7084**	**15**	**$3.75x10^7$**	**Estimate in ref 1.**
Thelon	0.16	0.7188	15	$2.40x10^6$	1
Kazan	0.26	0.7258	14	$3.64x10^6$	1
Winisk	0.25	0.7177	13	$3.25x10^6$	1
Moisie	0.14	0.7163	13	$1.82x10^6$	1
Aux Outardes	0.10	0.7186	12	$1.20x10^6$	1
Hudson	1.45	0.7118	12	$1.74x10^7$	1
Arnaud	0.09	0.7264	11	$9.90\ x10^5$	1
Hayes	0.41	0.7177	11	$4.51x10^6$	1
Natashquan	0.14	0.7131	11	$1.54x10^6$	1
Attawapiskat	0.30	0.7140	9	$2.70x10^6$	1
Avon	33.55	0.7326	0.3	$1.01x10^7$	1
Tamar	0.93	0.7098	0.2	$1.86x10^5$	1
Total - glaciated		**0.71177**	**3756**	**$4.89\ x10^9$**	**23% of global Sr flux**
Total - all		**0.71144**	**23966**	**$2.16\ x10^{10}$**	
Global riverine flux		**0.71144**		**$3.37\ x10^{10}$**	

[1] Compilation covers about 64% of global water discharge. Estimates for some rivers are given in bold type. Note that omission of all the estimates in this compilation has minimal impact on the hydrothermal Sr flux required by the global riverine flux - changing it by 1%.
[2] Where two measurements for one river are available, usually from ref 1 and either ref 2 or 9, an average is given here. The maximum impact of using only one of those measurements on the global riverine flux is ±0.00005 on $^{87}Sr/^{86}Sr$ and ±2% on the total Sr flux.

[3] Of the few new rivers in this compilation, only the Lena has a significant impact on the global riverine flux. Without the Lena the global riverine flux has an $^{87}Sr/^{86}Sr$ 0.00017 higher, with an insignificant change in the total Sr flux.
[4] Discharges from ref 1 if in their compilation, from ref 2 if not. From other sources where specified.
[5] Sr flux calculated from discharge and measured Sr concentration, except for the Ganges-Brahmaputra system for which ref 3 gives a seasonally-averaged total Sr flux and $^{87}Sr/^{86}Sr$ ratio.
[6] Meghna discharge from ref 6. Note that ref 4 gives $^{87}Sr/^{86}Sr$ as 0.723 and discharge of 1003 km^3/yr for the Meghna. This already includes components of the Ganges and Brahmaputra flow, which are here listed separately (A. Galy, pers. comm. 2007).
[7] Sr concentration is an estimate from ref 1.
[8] See text. We divide rivers into those draining regions that were/were not glaciated during the Pleistocene.
[9] Estimate - assumed to be same as Baltic rivers in ref 8.

Table S2: Sensitivity of calculated required high-temperature hydrothermal water flux to different versions of the global riverine Sr flux.

	Riverine flux		Required high-T hydrothermal water flux (kg/yr)[1]	Fraction of value using rivers as ref 1
	Total Sr flux (mol/yr)	$^{87}Sr/^{86}Sr$		
Compilation ref 1[2]	3.03×10^{10}	0.71199	1.27×10^{14}	
As ref 1 but with Ganges-Brahmaputra from ref 3.	2.92×10^{10}	0.71177	1.11×10^{14}	0.88
As ref 1 but with November Ganges from ref 10[3].	3.08×10^{10}	0.71233	1.46×10^{14}	1.16
As ref 1 but with June Ganges from ref 10.	2.99×10^{10}	0.71169	1.10×10^{14}	0.87
As ref 1 but with January Brahmaputra from ref 11[4].	3.09×10^{10}	0.71231	1.46×10^{14}	1.15
As ref 1 but with May Brahmaputra from ref 11.	3.01×10^{10}	0.71192	1.22×10^{14}	0.96
New compilation (Table S1)	3.37×10^{10}	0.71144	1.11×10^{14}	0.88
New compilation with no estimates	3.44×10^{10}	0.71137	1.11×10^{14}	0.87

[1] Required hydrothermal water flux given the specified riverine fluxes, the diagenetic Sr flux and its isotopic composition used in ref 1, to produce a $d(^{87}Sr/^{86}Sr)/dt = 5.4 \times 10^{-5}$/Myr, the rate of increase for the modern oceans (ref 12 and equation S1 later in the supplementary material. The Sr isotopic composition of the basaltic Sr flux (0.7025) and the Sr concentration in the hydrothermal fluid (90 μmol/kg) are as used in ref 13.

[2] Some rivers updated using new data in ref 2.

[3] Our aim here is to assess the sensitivity of the required hydrothermal flux to uncertainties in the size and isotopic composition of the riverine Sr flux due to the fact that generally only one measurement is available from many rivers despite the fact that rivers are seasonal. Seasonal data are available from two prominent rivers – the Ganges and Brahmaputra – that exhibit extreme seasonality in runoff and weathering characteristics. Data from ref 10 is not from the Ganges mouth. The approach taken here, to obtain an estimate of the impact of seasonal variation in riverine Sr characteristics, is to modify the Ganges data in ref 1 to reflect the seasonal variation seen in ref 10. The months chosen, November and June, are those for which the $^{87}Sr/^{86}Sr$ and Sr concentration of the river would impart the maximum and minimum forcing of seawater $^{87}Sr/^{86}Sr$. The annual discharge-weighted average for the river is calculated using the data in ref 10. Then the fractional difference between this value and the two most extreme months is calculated for Sr concentration and $^{87}Sr/^{86}Sr$. Then the values in ref 1 are modified by these amounts and applied to the entire annual discharge and a new global riverine flux calculated. The calculation illustrates that one unrepresentative measurement from this river would impact the required hydrothermal water flux at the 10-15% level, and certainly cannot explain the gross imbalance in the oceanic Sr budget.

[4] As above but for the Brahmaputra data in ref 11.

Table S3: Biotite $^{87}Sr/^{86}Sr$ data and constraints on potential size of incongruent weathering effect in young mountain belts on riverine Sr isotope flux.

Location	Whole rock	Feldspar	Biotite	Shift in %	Modern weathering	Modern weathering shift as % of total biotite-bulk rock difference	Data source
Wyoming soils B horizon[1]	0.722577		1.13	56.38	0.7265	0.96	14
Location	Whole rock	Feldspar	Biotite	Shift in %[2]	Modeled modern weathering[3]	Modeled % shift from bulk rock[4]	Data source
Zanskar Himalaya		0.757743	0.801733	5.81	0.758167	0.06	15
		0.765727	0.814839	6.41	0.766200	0.06	
		0.715637	0.730499	2.08	0.715780	0.02	
		0.726043	0.781588	7.65	0.726578	0.07	
Nepalese Himalaya		0.80081	0.88841	10.94	0.801653	0.11	16
	0.79706		0.84304	5.77	0.797503	0.06	
Garhwal Himalaya		0.7157	0.9235	29.03	0.717701	0.28	17
Nepalese Himalaya	0.7741		1.0082	30.24	0.776354	0.29	18
	0.8545		0.9553	11.80	0.855471	0.11	
	0.813		0.8304	2.14	0.813168	0.02	
	0.8468		0.9201	8.66	0.847506	0.08	
	0.9297		1.1152	19.95	0.931486	0.19	
	0.7629		0.9761	27.95	0.764953	0.27	
	0.7547		0.846	12.10	0.755579	0.12	
Swiss Alps	0.7172		0.7500	4.57	0.717516	0.04	19
	0.7284		0.8297	13.91	0.729375	0.13	
	0.7126		0.8045	12.90	0.713485	0.12	
	0.7664		1.2450	62.45	0.771008	0.60	
	0.7664		1.5020	95.98	0.773483	0.92	
	0.7085		0.7922	11.81	0.709306	0.11	
	0.7091		0.8109	14.36	0.710080	0.14	
	0.7169		0.8207	14.48	0.717899	0.14	
	0.7105		0.7884	10.96	0.711250	0.11	
	0.7116		0.7821	9.91	0.712279	0.10	
	0.7090		0.8619	21.57	0.710472	0.21	
	0.7090		0.8256	16.45	0.710123	0.16	
	0.7090		0.8006	12.92	0.709882	0.12	
	0.7102		0.7807	9.93	0.710879	0.10	
	0.7080		0.7392	4.41	0.708300	0.04	
	0.7079		0.7440	5.10	0.708248	0.05	
	0.7145		0.8827	23.54	0.716120	0.23	
	0.7177		0.8827	22.99	0.719289	0.22	
	0.8261		2.2610	173.70	0.839916	1.67	
	0.8261		1.9790	139.56	0.837201	1.34	
	0.7122		0.7685	7.91	0.712742	0.08	
	0.7170		0.7590	5.86	0.717404	0.06	
	0.7376		1.5080	104.45	0.745018	1.01	
Average				26.5		0.26	
Low				2.1		0.02	
High				174		1.67	
Likely % global shift from whole rock in weathering flux $^{87}Sr/^{86}Sr$ from whole rock[5]						0.33	

[1] Data from Wyoming soils. Biotite and whole rock for B horizon as measured in Blum and Erel[14]. Modern flux of $^{87}Sr/^{86}Sr$ due to weathering from the model described later in supplemental material. Note that the shift from the whole soil value produced by the model is a minimum, leading to minima for estimated effect of incongruent weathering of Himalayan and Alpine rocks further down the table, as local streams have $^{87}Sr/^{86}Sr$ even further in excess of the bulk soils (= 0.739-0.743).

[2] % shift in biotite $^{87}Sr/^{86}Sr$ from whole rock or feldspar.

[3] Modeled modern weathering flux of $^{87}Sr/^{86}Sr$ making the assumption that the shift of the present-day weathering flux from the whole rock (or feldspar) is the same proportion of the shift in $^{87}Sr/^{86}Sr$ between whole rock and biotite as for the Wyoming samples.

[4] Modern weathering flux of $^{87}Sr/^{86}Sr$ expressed as a percentage difference from the whole rock (or feldspar).

[5] Calculated given the data for Precambrian Wyoming soils (representative of high-latitude glaciated regions) and that for non-glaciated regions above. This value is dominated by the latter because only 10% of the silicate Sr flux to the oceans derives from the glaciated regions (Table S1 and the amount of silicate weathering expressed as a fraction of the total =14%[2]) for the high-latitude regions.

Model details

Chemical weathering rate variations with time

We contend that chemical weathering rates on the modern Earth are faster than over timescales of 10^5 yrs, and much faster than over timescales of 10^7 yrs. Our bases for this proposition are the fact that chemical weathering rates are strongly dependent on the age of the substrate being weathered (the time it has been exposed to chemical weathering), the seemingly unavoidable conclusion that the average age of substrates decreased dramatically at the last deglaciation and previous deglaciations, and the proposition that the modern weathering flux as estimated from rivers continues to be out of steady-state. We can quantify the extent of this disequilibrium if we know the dependence of chemical weathering rate on substrate age and if we have constraints on the age distribution of new substrate exposed from underneath the ice during the deglaciation (the high latitude glaciated regions, and at lower latitudes where mountain glaciers were significant during the last glaciation and are now much less so – e.g. the European Alps, the Andes), or produced during the deglaciation by increased pulses of physical weathering in regions such as the Himalaya, Alps, Andes etc. The dependence of chemical weathering rate on substrate age is quantified in Figure 2 of the paper, where the exponent in the power law relationships remains constant over a wide range of climate regimes (e.g. the cold temperate climate of Wyoming versus the tropical climate of Hawaii) and between granitic and basaltic lithologies. Quantitative limits on the exposure of new substrate from beneath ice-sheets are available from a range of constraints on the extent of ice-sheet coverage during recent glaciations. The timing of production of new substrate outside the glaciated regions is often relatively precise, but the amount produced and the balance between new substrate and old in the weathering regime is much more difficult to assess.

A key component of our hypothesis is that the disequilibrium in modern weathering rates applies only to silicate weathering, because fast reaction kinetics for carbonate weathering keep physical and chemical weathering rates much closer to equilibrium with each other. We note that our general approach to quantifying changes in silicate weathering rates in the glaciated regions is very similar to that of Clark et al.[20], based on data in various previous publications by Blum and others[14,21]. Similarly, our assumption that carbonate weathering rates are not sensitive to changes in environmental parameters, but keep pace with physical weathering, was also made be these authors.

The modeling approach used to simulate potential changes in silicate chemical weathering rates at high latitudes in response to glacial-interglacial climate change is similar to that used by Foster and Vance[22] to model changes in North Atlantic Pb isotopes. In the following the "glaciated region" refers to those parts of the high-latitudes continents that, over the last glacial cycle, were at some stage covered by ice. Chemical weathering rate beneath the ice was assumed to be negligible[23-25] and in front of the ice sheet, but within the "glaciated region", was modeled as dependent on substrate age, as in Figure 2 of the paper. Substrate age is the time since ice last covered that location. The proportion of the glaciated region covered by ice at any one time was assumed to vary linearly with $\delta^{18}O$[26] between values of 0 (none of the glaciated region covered in ice) and 1 (all of it covered in ice) and the retreat and advance of ice sheets was simulated at 1 kyr resolution. A linear relationship between $\delta^{18}O$ (~ice volume) and the area covered by an ice-cap is clearly an over-simplification, but such a consideration is of only minor importance here. For each 1 kyr interval, the total area of glaciated region in front of the ice sheet at that time is split into age bins spaced at 1 kyr, corresponding to the time elapsed since it was last covered by ice. Then the average chemical weathering rate for the area exposed to chemical weathering is calculated using the relationships in Figure 2[21,27,28], ie. instantaneous weathering rate = $50e^{xt}$. The thickness of the curve yielding chemical weathering rate through time in Figure 2 reflects the fact that the exponential constant (x) is found to be -0.71 for post-glacial soils from a range of locations[25] while the value for both laboratory experiments on Panola granite[26] and field studies of basalts of varying eruption ages[27] is -0.61. We note that the nature of the time-dependency of weathering rate is the same in all three published studies used in Figure 2. This is the case despite the very different environments (cold, dry, temperate vs wet tropical vs laboratory conditions), the different rock types (granite, granitoid moraine, basalt) involved, and the very different absolute weathering rates in each environment, which we are not concerned with here. Because the original studies did not supply uncertainties on individual data points, it is difficult to produce a statistically rigorous estimate of uncertainty on the slope of a putative universal relationship that would describe the time-dependency of weathering rates for all three studies. We argue, however, that the difference – or in this case striking similarity

– between the time-dependency of weathering rate as expressed in the slopes of the relationships in Figure 2 of the paper, gives us an adequate estimate for our purposes here of the uncertainty on the single slope that would describe all the data if absolute changes in weathering rate across the three studies were taken into account.

Clarke et al.[20] use very similar relationships for the dependence of weathering rate on substrate age – both our approaches are based on data in work by Blum and others[14,21] – and the deglacial pulses in weathering rate that they simulate are quantitatively very similar to those produced here. The main difference is that their pre-exponent in the power law relationship for instantaneous weathering rate in the high-latitude regions is 72 instead of our value of 50. A value of 50 is obtained by re-calculating the chemical weathering data in Taylor and Blum[21], in eq m^{-2} kyr^{-1}, to mol m^{-2} kyr^{-1} using the chemical composition of the Wyoming soils studied. The Clark et al.[20] value of 72 was adjusted from the above to match modern weathering rates with those of Millot et al.[29] in modern Canada. But the pre-exponent is immaterial to us here as we are interested purely in changes in weathering rate with substrate age.

The application of these concepts to regions of the Earth, like the Himalaya, where deglaciation is not the main driver of changes in substrate age but where large monsoon-driven increases in physical weathering produced massive amounts of new substrate, is much more difficult to model quantitatively. The power law dependence of weathering rate on substrate age, given the studies of Hawaiian soils in Porder et al.[28] and the laboratory experiments in White and Brantley[27], is robust across a wide range of climate regimes and lithologies. The issue is how to quantitatively model the production of new substrate. Our approach in the paper is to extend the constraints from the glaciated regions and to assess the impact of such a model on the delivery of Sr and its isotopes to the oceans. The quantitative constraints that arise can then be tested using other elements.

Models of total Sr and Sr isotopes in the riverine flux to the oceans (Fig. 4 of paper)

All calculations used as a starting point the following parameters:

Modern seawater $^{87}Sr/^{86}Sr$:	0.70917[12]
Modern seawater Sr inventory:	1.25×10^{17} mol
$d(^{87}Sr/^{86}Sr)/dt$ for past 2-3 Myr	0.000054 Myr^{-1} (ref 12)
Modern global riverine $^{87}Sr/^{86}Sr$:	0.71144 (Table S1)
Modern global riverine Sr flux:	3.37×10^{10} mol yr^{-1} (Table S1)
Modern riverine $^{87}Sr/^{86}Sr$ for glaciated regions:	0.71177 (Table S1)
Modern riverine Sr flux for glaciated regions:	0.77×10^{10} mol yr^{-1} (Table S1)
Modern riverine $^{87}Sr/^{86}Sr$ for non-glaciated regions:	0.71134 (Table S1)
Modern riverine Sr flux for non- glaciated regions:	2.60×10^{10} mol yr^{-1} (Table S1)
Hydrothermal $^{87}Sr/^{86}Sr$	0.7025[13]
Diagenetic flux $^{87}Sr/^{86}Sr$:	0.7084[1,30]
Diagenetic Sr flux:	0.34×10^{10} mol yr^{-1} (refs 1,30)

The Sr mass balance for the ocean is as follows[13]:

$d(^{87}Sr/^{86}Sr)/dt = 0.000054\ Myr^{-1} =$

$$F_{river}\left[\frac{\left(\frac{^{87}Sr}{^{86}Sr}\right)_{river}-\left(\frac{^{87}Sr}{^{86}Sr}\right)_{sw}}{Sr_{SW}}\right]+F_{hydr}\left[\frac{\left(\frac{^{87}Sr}{^{86}Sr}\right)_{hyd}-\left(\frac{^{87}Sr}{^{86}Sr}\right)_{sw}}{Sr_{SW}}\right]+F_{diag}\left[\frac{\left(\frac{^{87}Sr}{^{86}Sr}\right)_{diag}-\left(\frac{^{87}Sr}{^{86}Sr}\right)_{sw}}{Sr_{SW}}\right] \quad \text{(S1)}$$

where $F_{river,hyd,diag}$ is the total Sr flux from rivers, hydrothermal systems or the diagenetic back flux from deep-sea sediments, $(^{87}Sr/^{86}Sr)_{rivers,hyd,diag}$ is the corresponding Sr isotopic compositions and Sr_{SW} and $(^{87}Sr/^{86}Sr)_{sw}$ is the total inventory of Sr, and its isotopic composition, in modern seawater.

This cannot be solved for the present-day with a reasonable hydrothermal flux if modern rivers are regarded as accurately representing the long-term flux of Sr and its isotopes to the oceans. With a long-term riverine flux that is the same as modern rivers, and with a hydrothermal flux[13] and the smaller diagenetic flux[30] as suggested by various independent constraints, the $^{87}Sr/^{86}Sr$ of seawater should have evolved at a rate of 0.000425 Myr^{-1} over the Quaternary. The observed rate of increase is some 8 times slower – at 0.000054 Myr^{-1}. Stoll and Schrag[31] have suggested that sea-level low stands during glacial periods leads to an increased flux of Sr to the oceans from carbonates, both by dissolution of shelf carbonate and by the re-crystallisation of aragonite (holding higher concentrations of Sr) to calcite (with lower concentrations of Sr). We have taken such a phenomenon into account in our models, as a possible explanation for the slow evolution observed in seawater records, by simulating a 10-fold increase in the diagenetic flux of Sr from carbonates for the roughly 70% of the past 400 kyr when the Northern Hemisphere was glaciated. Such an approach generates an increased Sr flux to the oceans that is, over and entire glacial cycle, roughly equivalent to that considered by Stoll and Schrag[31]. However, the simulation that takes this factor into account produces an evolution in seawater Sr isotopes that is still 6 times faster than observed in the data. Furthermore, the impact of this extra unradiogenic Sr in our models is over-estimated, because we assume that the isotopic composition of that flux is the same as that estimated by Elderfield and Gieskes[30] for the background diagenetic flux (0.7084). The increased flux from shelves during glacials in the Quaternary will be much closer to the seawater value and will have a much smaller impact on seawater Sr isotopes as a result, but the approach of simulating the effect of the least unradiogenic Sr possible serves to set a lower bound on the amount of the silicate flux that is currently out of steady-state and variable during Quaternary glacial-interglacial cycles (see below).

Figure 4 provides an illustrative simulation of the time evolution of oceanic Sr isotopes over the past 400 kyr with variable chemical weathering rates (and thus Sr flux) and variable $^{87}Sr/^{86}Sr$ in a fraction of the silicate portion of the riverine Sr flux. In all simulations in Figure 4, the hydrothermal flux is held constant at the best-estimate values in Davis et al.[13]. The modern riverine flux of Sr is partitioned into a carbonate portion (70% of the Sr) with an $^{87}Sr/^{86}Sr$ of 0.708 (close to the average for Phanerozoic limestones) that is also kept constant, and a total silicate portion with a modern $^{87}Sr/^{86}Sr$ obtained by mass balance, given the constraint that the total riverine flux must have a modern $^{87}Sr/^{86}Sr = 0.71144$ (Table S1).

The total silicate flux is then further split into a portion affected by non-steady-state processes (0% (or "modern riverine flux" on Fig. 4), 40% and 70% of the total silicate flux as labeled on the curves in Figure 4), and an unaffected portion (100%, 60% or 30% of the total silicate flux). The non-steady-state portion of the silicate flux is allowed to vary in magnitude and in isotopic composition through glacial-interglacial climate cycles. For this portion, the flux of Sr is assumed to vary according to Figure 3, with new substrate produced at each deglaciation such that weathering rates are reset to high values. $^{87}Sr/^{86}Sr$ is also assumed to change with soil age due to incongruent weathering of Sr. The two main pieces of evidence for this, and its dependence on substrate age, are summarized in Figure S1. The data in Figure S1a suggest that modern chemical weathering of Precambrian terrains is releasing Sr that is different from the bulk material available for weathering long-term by 1-4%. As noted in Table S3, such a process also likely applies to non-glaciated terrains but at a more subtle level (perhaps 0.25% on average, Table S3) because the biotites that release the anomalously radiogenic Sr are younger, particularly in the mountain belts that supply large amounts of Sr to the oceans and which are also most likely to be out of steady-state. Figure 4 uses values of 0.2-0.4% (see Table S3) for the present-day deviation of $^{87}Sr/^{86}Sr$ from bulk soil, and a dependence on time given by the slope of Figure S1 (see below). As for the Sr flux, the isotopic

composition is reset at each deglaciation. The output flux is fixed at the average of the total input flux to maintain long-term oceanic balance through glacial-interglacial cycles. This may not be valid but is largely irrelevant here.

Our quantitative approach to modeling the incongruent weathering of Sr and its dependence on substrate age derives principally from the measurements in a Wyoming soil chronosequence. The validity of the work of Blum and co-workers on these soils[14,21] has been called into question in a comment on one of the original papers. Dahms et al.[33] suggest that the variation in weathering rate with soil age obtained by Taylor and Blum[21] was compromised by the possible addition of airborne dust to the older soils. The good agreement between the power law relationship obtained by Taylor and Blum[21] for the dependence of weathering rate on substrate age with those from both laboratory experiments and the Hawaiian chronosequence argues against the significance of such a complication. Moreover, and as noted in a reply by Taylor and Blum[34] in a reply to the Dahms et al.[33] comment, a maximum of 2-5% of the minerals in the Wyoming soils is likely to be aeolian. Most importantly for our paper, the reply also points out that there is little detectable shift in the bulk $^{87}Sr/^{86}Sr$ of the <2mm fraction of the B versus the C horizons of each soil, suggesting that the B horizon does not contain any significant aeolian input given that the unradiogenic Sr that is supposedly added has an $^{87}Sr/^{86}Sr$ of 0.705 versus ratios in Wind River rocks of 0.725. Another potential caveat is the possible addition of carbonate dust to the older soils as they age (e.g. ref. 35). Such a process could, in principle, contribute to the relationship between soil age and $^{87}Sr/^{86}Sr$. However, such an explanation for the Sr isotopes would leave the documented relationship between soil age and Pb isotopes – Pb being a much more minor component of carbonate and insignificant to the Pb budget of the soils – as co-incidental. Furthermore, it is not clear how long carbonate would survive in the acidic environments of these soils.

The soil systematics are not the only argument we invoke in support of our models. We also point to the leaching experiments that have been done on granites by Erel et al. (2004)[32] (Fig. S1b), which show that both radiogenic Sr and radiogenic Pb are released by "early" weathering of granitoid rocks as (admittedly crudely) simulated by the leaching experiments. Finally, our models do not rely on the exact figures in the Wyoming papers. Indeed, in calculating the impact of incongruent weathering on the global Sr flux we scale these numbers down to those that might be relevant to much younger rocks containing pools of much less radiogenic Sr – such as those that might characterize the Himalaya, the Alps, or other young mountain belts.

All of the illustrated model evolutions are set to arrive at the $^{87}Sr/^{86}Sr$ of modern seawater (~0.70917). The difference between them is the rate at which they get there. Figure 4 shows that the rate of increase is 8 times too fast if modern rivers are regarded as representative of the long-term chemical weathering flux. It is also too fast if as little as 40% of the total silicate flux is out of steady state as above. But if 70% of the silicate flux is out of steady state, the resultant riverine flux results in a rate of increase in seawater that matches well with data. The glacial-interglacial cyclicity in the riverine flux we invoke induces cyclicity in seawater Sr isotopes, but the cyclicity induced is not great enough to be inconsistent with the highest precision data we have for seawater Sr at this stage (Fig. 4).

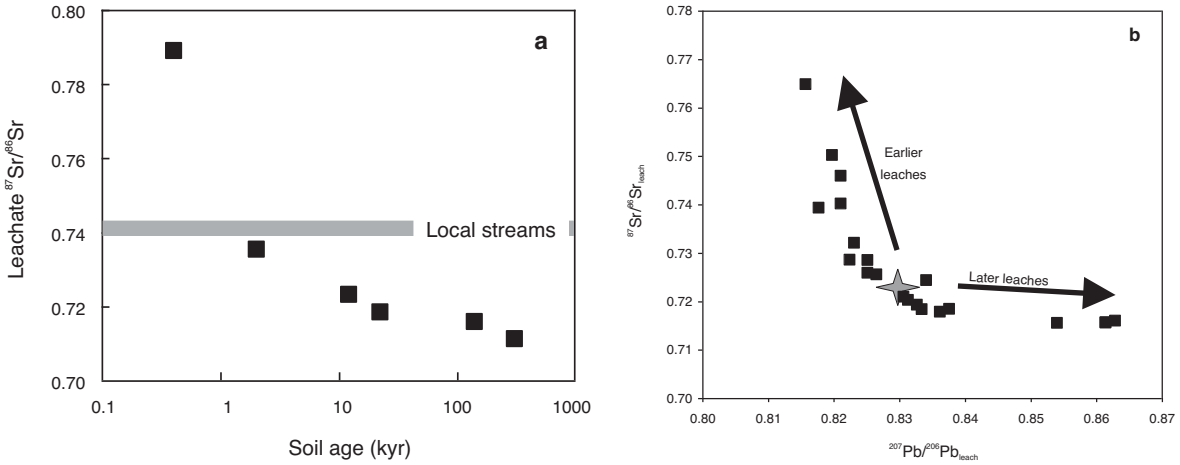

Figure S1:

a. Sr data for weak leaches of the B horizons of soils in a chronosequence from Wyoming, USA[14]. Soil age reflects the time since exposure from underneath an ice-sheet. Leaches of soils that were exposed at the last deglaciation are about 0.9% more radiogenic than the whole rock. Sr in local streams is up to 4% more radiogenic than local bulk rocks. The former value is used here as a measure of the anomaly in the Sr being released from the recently glaciated Precambrian shields (for Figure 4 in the paper). The time evolution of the isotopic composition of B horizon Sr in this figure is used to simulate the temporal variability of the riverine flux in an illustrative model of Sr isotopic evolution in the oceans over the past 400 kyr (Figure 4 in the paper).

b. Pb and Sr isotopic compositions of weak acid (pH 1) leaches of the Elat granite (squares) as compared with it's whole rock isotopic composition (grey star)[32], to simulate the effect of weathering release of Sr and Pb The evolution of radiogenic Pb by early leachates explains the radiogenic ratios seen during interglacial periods in records of deep Atlantic Pb[22]. This radiogenic Pb is clearly accompanied by Sr more radiogenic than the whole rock.

Supplementary references:

1. Palmer, M.R. & Edmond, J.M. The strontium isotope budget of the modern ocean. *Earth Planet. Sci. Lett.* 92, 11-26 (1989).
2. Gaillardet, J., Dupré, B., Louvat, P. & Allègre, C.J. Global silicate weathering and CO2 consumption rates deduced from the chemistry of large rivers. *Chem. Geol.* 159, 3-30 (1999).
3. Galy, A. France-Lanord, C. & Derry, L.A. The strontium isotopic budget of Himalayan Rivers in Nepal and Bangladesh. *Geochim. Cosmochim. Acta* 63, 1905-1925 (1999).
4. Tipper, E.T. et al. The magnesium isotope budget of the modern ocean: Constraints from riverine magnesium isotope ratios. *Earth Planet. Sci. Lett.* 250, 241-253 (2006).
5. Huh, Y., Panteleyev, G., Babich, D., Zaitsev, A. & Edmond, J.M. The fluvial geochemistry of the rivers of Eastern Siberia: III. Tributaries of the Lena and Anabar draining the basement terrain of the Siberian Craton and the Trans-Baikal Highlands. *Geochim. Cosmochim. Acta* 63, 967-987 (1998).
6. Mikhailov, V.N. & Dotsenko, M.A. Peculiarities of the hydrological regimes of the Ganges and Brahmaputra River mouth area. *Water Res.* 33, 389-409 (2006).
7. Moon, S., Huh, Y., Qin, J. & van Pho, N. Chemical weathering of the Hong (Red) River basin: rates of silicate weathering and their controlling factors. *Geochim. Cosmochim. Acta* 71, 1411-1430 (2007).
8. Löfvendahl, R., Aberg, G. & Hamilton, P.J. Strontium in rivers of the Baltic Basin. *Aquatic Sci.* 52, 315-329 (1990).
9. Millot, R., Gaillardet, J., Dupré, B. & Allègre, C.J. Northern latitude weathering rates: clues from the Mackenzie River Basin, Canada. *Geochim. Cosmochim. Acta* 67, 1305-1329 (2003).
10. Bickle, M.J. et al. Fluxes of Sr into the headwaters of the Ganges. *Geochim. Cosmochim. Acta* 67, 2567-2584 (2003)
11. Rai, S.K. & Singh, S.K. Temporal variation in Sr and $^{87}Sr/^{86}Sr$ of the Brahmaputra: implications for annual fluxes and tracking flash floods through chemical and isotopic composition. *Geochem. Geophys. Geosyst.* 8, Q08008, 10.1029/2007GC001610 (2007).
12. Hodell, D.A., Mead, G.A. & Mueller, P.A. Variation in the strontium isotopic budget of seawater (8 Ma to present): implications for chemical weathering rates and dissolved fluxes to the oceans. *Chem. Geol.* 80, 291-307 (1990).
13. Davis, A.C., Bickle, M.J. & Teagle, D.A.H. Imbalance in the oceanic strontium budget. *Earth Planet. Sci. Lett.* 211, 173-187 (2003).
14 Blum, J.D. & Erel, Y. Rb-Sr isotope systematics of a granitic soil chronosequence: the importance of biotite weathering. *Geochim. Cosmochim. Acta* 61, 3193-3204 (1997).
15. Inger S. Timing of an extensional detachment during convergent orogeny: new Rb-Sr geochronological data for the Zanskar Shear Zone, northwestern Himalaya. Geology 26, 223-226 (1998).
16. Johnson, M.R.W. & Rogers, G. Rb-Sr ages of micas from the Kathmandu Complex, central Nepalese Himalaya: implications for the evolution of the Main Central Thrust. *J. Geol. Soc. London* 154, 862-869 (1997)
17. Bickle, M.J. et al. Controls on the 87Sr/86Sr ratio of carbonates in the Garhwal Himalaya, headwaters of the Ganges. *J. Geology* 109, 737-753 (2001).
18. Kai, K. & Hayase, I. Rb-Sr age and initial Sr isotopic ratio of some Himalayan rocks. *J. Mass Spectrom. Soc. Japan* 24, 181-188 (1976).
19. Hurford, A.J. Cooling and uplift patterns in the Lepontine Alps South Central Swizerland and an age of vertical movement on the Insubric Line. *Contrib. Mineral. Petrol.* 92, 413-427 (1986).
20. Clark, P.U. et al. The middle Pleistocene transition: characteristics, mechanisms and implications for long-term changes in atmospheric CO_2. *Quat. Sci. Rev.* 25, 3150-3184 (2006).
21. Taylor, A. & Blum, J.D. Relation between soil age and silicate weathering rates determined from the chemical evolution of a glacial chronosequence. *Geology* 23, 979-982 (1995).
22. Foster, G.L. & Vance, D. Negligible glacial-interglacial variation in continental chemical weathering rates. *Nature* 444, 918-921 (2006).
23. Kump, L.R. & Alley, R.B. in *Material Fluxes on the Surface of the Earth* (eds Usselman, T.M. & Hay, W.W.) 46-40 (National Academy Press, Washington DC, 1994).
24. Tranter, M. et al. Direct effect of ice-sheets on terrestrial bicarbonate, sulphate and base cation fluxes during the last glacial cycle: minimal impact on atmospheric CO_2 concentrations. *Chem. Geol.* 190, 33-44 (2002).
25. Anderson, S.P. Biogeochemistry of glacial landscape systems. *Annu. Rev. Earth Planet. Sci.* 35, 375-399 (2007).

26. Imbrie, J. et al. in Milankovitch and Climate (eds Berger, A. L., Imbrie, J., Hays, J., Kukla, G. & Saltzmen, B.) 269–305 (Reidel, Dordrecht, 1984).
27. White, A.F. & Brantley, S.L. The effect of time on the weathering of silicate minerals: why do weathering rates differe in the laboratory and the field. *Chem. Geol.* 202, 479-506 (2003).
28. Porder, S., Hilley, G.E. & Chadwick, O.A. Chemical weathering, mass loss, and dust inputs across a climate by time matrix in the Hawaiian Islands. *Earth Planet. Sci. Lett.* 258, 414-427 (2007).
29. Millot, R., Gaillardet, J., Dupré, B. & Allègre, C.J. The global control of silicate weathering rates and the coupling with physical erosion: new insights from rivers of the Canadian Shield. *Earth Planet. Sci. Lett.* 196, 83-98 (2002).
30. Elderfield, H. and Gieskes, J.M. Sr isotopes in interstitial waters of marine sediments from Deep Sea Drilling Project cores. *Nature* 300, 493-497 (1982).
31. Stoll, H.M. and Schrag, D.P. (1998) Effect of Quaternary sea-level cycles on Sr in seawater. *Geochim. Cosmochim. Acta* 62, 1107-1118 (1998).
32. Erel, Y., Blum, J.D., Roueff, E. & Ganor, J. Lead and strontium isotopes as monitors of experimental granitoid mineral dissolution. *Geochim. Cosmochim. Acta* 68, 4649-4663 (2004).
33. Dahms, D.E. et al. Relation between soil age and silicate weathering rates determined from the chemical evolution of a glacial chronosequence: Comment. *Geology* 25, 381-382 (1997).
34. Taylor, A. and Blum, J.D. Relation between soil age and silicate weathering rates determined from the chemical evolution of a glacial chronosequence: Reply. Geology 25, 382-383 (1997).
35. Reheis, M.C. Influence of climate and eolian dust on the major-element chemistry and clay mineralogy of soils in the Northern Bighorn Basin, USA. Catena 17, 219-248 (1990).